Article

Temporal Dynamics of Global Barren Areas between 2001 and 2022 Derived from MODIS Land Cover Products

Marinos Eliades [1,2,*], Stelios Neophytides [1,2], Michalis Mavrovouniotis [1,2], Constantinos F. Panagiotou [1], Maria N. Anastasiadou [1,2], Ioannis Varvaris [1,2], Christiana Papoutsa [1,2], Felix Bachofer [3], Silas Michaelides [1,2] and Diofantos Hadjimitsis [1,2]

Citation: Eliades, M.; Neophytides, S.; Mavrovouniotis, M.; Panagiotou, C.F.; Anastasiadou, M.N.; Varvaris, I.; Papoutsa, C.; Bachofer, F.; Michaelides, S.; Hadjimitsis, D. Temporal Dynamics of Global Barren Areas between 2001 and 2022 Derived from MODIS Land Cover Products. *Remote Sens.* **2024**, *16*, 3317. https://doi.org/10.3390/rs16173317

Academic Editors: Dino Ienco and Gilberto Camara

Received: 26 June 2024
Revised: 8 August 2024
Accepted: 5 September 2024
Published: 7 September 2024

CC BY

[1] ERATOSTHENES Centre of Excellence, Limassol 3012, Cyprus; stelios.neophytides@eratosthenes.org.cy (S.N.); michalis.mavrovouniotis@eratosthenes.org.cy (M.M.); constantinos.panagiotou@eratosthenes.org.cy (C.F.P.); maria.anastasiadou@eratosthenes.org.cy (M.N.A.); ioannis.varvaris@eratosthenes.org.cy (I.V.); christiana.papoutsa@eratosthenes.org.cy (C.P.); silas.michaelides@eratosthenes.org.cy (S.M.); d.hadjimitsis@eratosthenes.org.cy (D.H.)

[2] Remote Sensing and GeoEnvironment Lab, Department of Civil Engineering and Geomatics, Cyprus University of Technology, Limassol 3036, Cyprus

[3] Earth Observation Center (EOC), German Aerospace Center (DLR), 82234 Wessling, Germany; felix.bachofer@dlr.de

* Correspondence: marinos.eliades@eratosthenes.org.cy

Abstract: Long-term monitoring studies on the transition of different land cover units to barren areas are crucial to gain a better understanding of the potential challenges and threats that land surface ecosystems face. This study utilized the Moderate Resolution Imaging Spectroradiometer (MODIS) land cover products (MCD12C1) to conduct geospatial analysis based on the maximum extent (MaxE) concept, to assess the spatiotemporal changes in barren areas from 2001 to 2022, at global and continental scales. The MaxE area includes all the pixels across the entire period of observations where the barren land cover class was at least once present. The relative expansion or reduction of the barren areas can be directly assessed with MaxE, as any annual change observed in the barren distribution is comparable over the entire dataset. The global barren areas without any land change (UA) during this period were equivalent to 12.8% (18,875,284 km^2) of the global land surface area. Interannual land cover changes to barren areas occurred in an additional area of 3,438,959 km^2 (2.3% of the global area). Globally, barren areas show a gradual reduction from 2001 (91.1% of MaxE) to 2012 (86.8%), followed by annual fluctuations until 2022 (88.1%). These areas were mainly interchanging between open shrublands and grasslands. A relatively high transition between barren areas and permanent snow and ice is found in Europe and North America. The results show a 3.7% decrease in global barren areas from 2001 to 2022. Areas that are predominantly not barren account for 30.6% of the transitional areas (TAs), meaning that these areas experienced short-term or very recent transitions from other land cover classes to barren. Emerging barren areas hotspots were mainly found in the Mangystau region (Kazakhstan), Tibetan plateau, northern Greenland, and the Atlas Mountains (Morocco, Tunisia).

Keywords: land use/land cover; satellite; remote sensing; moderate resolution imaging spectroradiometer; geospatial analysis

monitoring studies on barren spatiotemporal dynamics are essential to better understand the potential challenges and threats facing land surface ecosystems.

Remote sensing techniques enable the monitoring of land surface at different spatiotemporal scales, providing valuable information on land cover and land changes [4]. Land cover data can be extracted from different satellite missions (e.g., Sentinel, Landsat, MODIS, AVHRR) that are currently available. Each mission offers unique advantages and disadvantages with respect to different resolutions and spatial and temporal coverages [5]. The data retrieved from these satellite missions have facilitated the development of various global land cover products with different spatial resolutions and classification systems [6–9]. According to Jing et al. [10], the Moderate Resolution Imaging Spectroradiometer (MODIS) land cover products are suitable for interannual land cover retrievals at a global scale due to their consistent data format and their long-term records.

1. Introduction

Barren land cover refers to regions with either sparse vegetation or bare soil, representing areas where either environmental constraints, climatic factors, or humanmade alterations of the environment are present, leading to unfavorable conditions for plant growth [1]. The transitional zones between barren and other land classes represent the threshold of the spatial expansion of vegetation [2]. Thus, these zones can be considered as critical indicators of terrestrial health [3]. As these areas evolve over time, long-term

Dynamic monitoring of spatiotemporal changes in land cover is crucial to gain better understanding of the impact of human and environmental processes on these changes [11–13]. Thus, there is a growing demand for tools that are capable for analyzing multidimensional data, defined as spatial data captured at multiple time instants. Towards this direction, many studies combined remote sensing data and Geographic Information Systems (GIS) [14–16]. The continuous enhancement of GIS with numerous geospatial algorithms has revolutionized the capabilities for satellite data analysis, as it enables the monitoring of land cover changes across various spatiotemporal scales in a repetitive and objective manner [17,18].

Monitoring the spatiotemporal dynamics of Earth's land cover is vital for assessing the impact of various processes over land surface, especially in the context of climate change and anthropogenic activities [8,19,20]. A recent study on global land use changes between 1960 and 2019 revealed that almost a third (32%) of the global land area [21] has been subjected to changes. According to the authors of that study, afforestation and cropland abandonment in the north hemisphere and deforestation and agricultural expansion in the south hemisphere are the main drivers of the observed land use changes. Liu et al. [22] reported statistical results of change detection of land surface at global and continental scales from 1982 to 2015, showing decreasing trends of barren areas in Africa, Asia, Europe, North America, and globally. More specifically, the authors found a decrease in barren land area in the Northern Hemisphere's middle and high latitudes, reflecting the increase in vegetation cover. In addition, no trends were found for South America and Australia. Wu et al. [23] found that the majority of the global barren areas did not exhibit non-trivial increasing trends in the past two decades, except some desert expansion hotspots found in Tunisia, Tajikistan, and Peru. According to Song et al. [24], global bare ground cover has decreased by 1.16 million km^2 from 1982 to 2016, most notably in agricultural regions in Asia. The authors highlighted the need to establish a multi-year library to assess the impact of interannual fluctuations in land change. Studies focusing exclusively on the systematic analysis of land cover dynamics of a certain land class (e.g., barren) at a global scale are essential to provide the necessary information for this purpose.

The main aim of this study is to analyze the spatiotemporal dynamics of barren area changes at global and continental scales. The specific objectives of this study are to (i) compute the annual changes of the global barren area, (ii) estimate the extent of the barren areas at a continental scale in relation to the maximum extent of the barren areas, and (iii) explore the annual land cover changes within the barren–vegetation transition zones.

The novelty of this study stems from the analysis of the spatiotemporal changes of barren areas relative to their maximum extent. The maximum extent concept includes all areas where barren areas were present across the entire period of observations. Thus, any annual change observed in the barren distribution is comparable over the entire dataset, allowing us to observe the relative expansion or reduction of the barren areas.

This study combines MODIS global (with 0.05 degrees spatial resolution) land cover data (MCD12C1) and the International Geosphere-Biosphere Programme (IGBP) classification schemes to analyze the global barren changes from 2001 to 2022. The outcomes of this study are expected to provide insights related to land cover spatiotemporal dynamics and to arid land research. This paper is organized as follows: the materials and methods are presented in Section 2; the results on the interannual spatial distribution and dynamics in global and continental barren land cover are presented in Section 3; the discussion on the key findings is provided in Section 4; and the concluding remarks are presented in Section 5.

2. Materials and Methods

2.1. Datasets

The Terra and Aqua combined Moderate Resolution Imaging Spectroradiometer (MODIS, NASA) Land Cover Climate Modeling Grid (CMG) (MCD12C1) Version 6.1 data with the International Geosphere-Biosphere Programme (IGBP) classification scheme were used in this study (https://lpdaac.usgs.gov/products/mcd12c1v061/, accessed on 16 November 2023). The IGBP land cover classification system partitions land cover into 17 classes (Table 1). The data are available from 2001 to 2022 at annual intervals with a 0.05-degree spatial resolution covering the entire globe, in HDF format (Hierarchical Data Format).

Table 1. International Geosphere-Biosphere Programme (IGBP) legend and class descriptions for the MCD12C1 products.

Name	Value	Description
Water Bodies	0	At least 60% of area is covered by permanent water bodies.
Evergreen Needleleaf Forests	1	Dominated by evergreen conifer trees (canopy >2 m). Tree cover >60%.
Evergreen Broadleaf Forests	2	Dominated by evergreen broadleaf and palmate trees (canopy >2 m). Tree cover >60%.
Deciduous Needleleaf Forests	3	Dominated by deciduous needleleaf (larch) trees (canopy >2 m). Tree cover >60%.
Deciduous Broadleaf Forests	4	Dominated by deciduous broadleaf trees (canopy >2 m). Tree cover >60%.
Mixed Forests	5	Dominated by neither deciduous nor evergreen (40–60% of each) tree type (canopy >2 m). Tree cover >60%.
Closed Shrublands	6	Dominated by woody perennials (1–2 m height) >60% cover.
Open Shrublands	7	Dominated by woody perennials (1–2 m height) 10–60% cover.
Woody Savannas	8	Tree cover 30–60% (canopy >2 m).
Savannas	9	Tree cover 10–30% (canopy >2 m).
Grasslands	10	Dominated by herbaceous annuals (<2 m).
Permanent Wetlands	11	Permanently inundated lands with 30–60% water cover and >10% vegetated cover.
Croplands	12	At least 60% of area is cultivated cropland.
Urban and Built-up Lands	13	At least 30% impervious surface area including building materials, asphalt, and vehicles.
Cropland/Natural Vegetation Mosaics	14	Mosaics of small-scale cultivation 40–60% with natural tree, shrub, or herbaceous vegetation.
Permanent Snow and Ice	15	At least 60% of area is covered by snow and ice for at least 10 months of the year.
Barren	16	At least 60% of area is non-vegetated barren (sand, rock, soil) or permanent snow and ice with less than 10% vegetation.

2.2. Research Methods

The MCD12C1 HDF data were imported and analyzed in ArcGIS® Pro (ESRI, Redlands, CA, USA). The methodological steps for the spatiotemporal analysis of the barren areas are presented in the relevant flow chart in Figure 1. A mosaic dataset was created, where all the HDF data were added, resulting in a multidimensional raster containing all the global land cover data between 2001 and 2022. The multidimensional raster was clipped by a global land surface polygon and subsetted for the "Majority Land Cover" variable (MLCT_1) from the MCD12C1 dataset, which shows the most likely IGBP class for each 0.05-degree pixel.

Figure 1. Flowchart showing the methodological steps for deriving the annual land cover changes, the spatial transitions of barren areas to other land cover classes, and the transition occurrence. MaxE is the maximum extent of barren areas, UA is the unchanged barren area, and TA is the transitional area. Yellow squares indicate the input data, whereas the arrows and the green squares indicate the main processing steps and approaches. Red squares indicate the main outputs.

The spatiotemporal distribution of the barren areas was created with the use of argument statistics by extracting the dimension value (year) at which the value "16" (Barren) was attained for each pixel in the multidimensional raster. To analyze the interannual dynamics of the barren areas, the upper boundary of their spatial distribution was first set by creating a single raster containing all the pixels where the value "16" appeared at least once between 2001 and 2022. This raster was converted to a polygon, and the polygon area that contains these pixels is defined as the "maximum extent" (MaxE) of the barren area. An additional raster was created that included the pixels containing the value "16" that did not change between 2001 and 2022. The polygon area that contains these pixels was defined as the "unchanged" barren area (UA). A polygon was created containing the "transitional" area (TA) from barren to another land class or vice versa by overlaying the maximum extent and unchanged polygons and extracting (clipping) their overlapping area.

The MaxE area polygon was used to clip the multidimensional raster. For the analysis at continental scales, the multidimensional raster was further clipped by the continent polygon surface areas. The annual extent of each land cover class within the MaxE area was computed, and annual histograms were created containing the pixel distributions (each bin was equal to a land cover class) from which the annual change and distribution of each value within the MaxE area were computed. The duration, first and last occurrence of barren areas were further examined by overlaying the annual raster data and creating the associated rasters. The transition occurrence (TO), which describes the degree of transitioning from barren to another land cover class (%) for each pixel, was computed as:

$$TO = \frac{(n - D)}{n} * 100 \quad (1)$$

where n is the study period (years), and D is the duration of barren presence (years).

The results on the annual transitions from barren to other land cover classes are presented as percentages of the MaxE area.

3. Results

3.1. Spatiotemporal Dynamics of Barren Areas

The global barren area for which no land changes (UAs) are observed during the period 2001–2022 was found to be 18,875,284 km^2, being equivalent to 12.8% of the global land surface area. Additionally, interannual land changes to barren areas and vice versa (TAs) occurred in an area of 3,438,959 km^2, representing about 2.3% of the global area, meaning that the global land surface area where barren land occurred at least once (MaxE) was 22,314,243 km^2 in total Globally, the largest areas of barren lands are located in the Arctic, Arabian Peninsula, Central and East Asia, and North Africa (Figure 2). Global barren areas remained relatively constant between 2001 (21,064,962 km^2) and 2009 (21,025,089 km^2), followed by a gradual decline between 2010 and 2022 (20,291,366 km^2) (Figure 3). The results suggested a 3.7% decrease of global barren areas for the period 2001 to 2022.

The annual spatial expansion of the barren areas was mainly observed at the edges of existing barren areas, ranging from ~5 km (pixel size) to 220 km in length per year. The emergence of new barren areas (first barren occurrence) was relatively higher between 2001 and 2004. The highest reduction in barren areas was found to be 368,447 km^2 in 2001. The first barren occurrence in 2022 was 27,903 km^2, showing the largest barren expansion since 2015, in areas predominantly occupied by other land cover classes. The spatiotemporal analysis revealed a local expansion of barren areas for 2022 in a region within Atlas Mountains, between Morocco and Algeria. Also, two emerging barren area hotspots were identified in the Mangystau region (Kazakhstan) and Tibetan plateau. Finally, an increase in the barren areas in northern Greenland was observed in the same year.

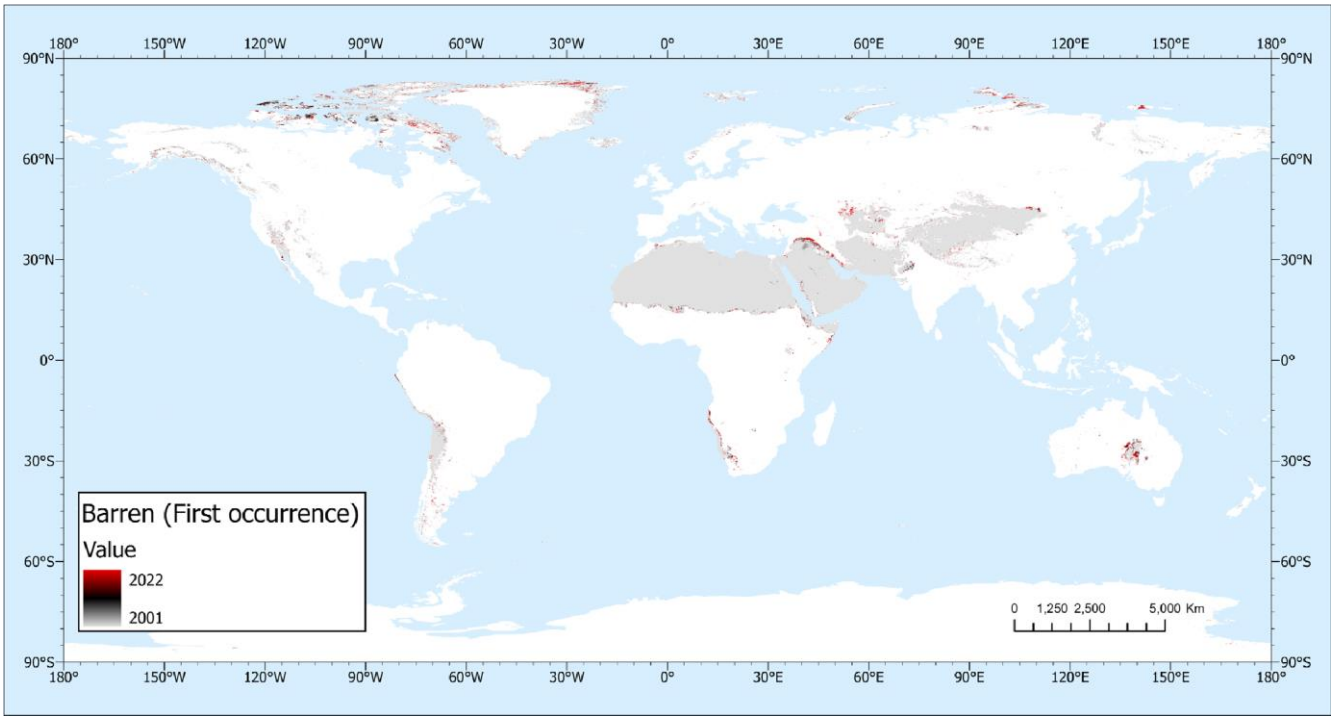

Figure 2. Spatial extent of the first occurrence of the barren areas per year between 2001 and 2022.

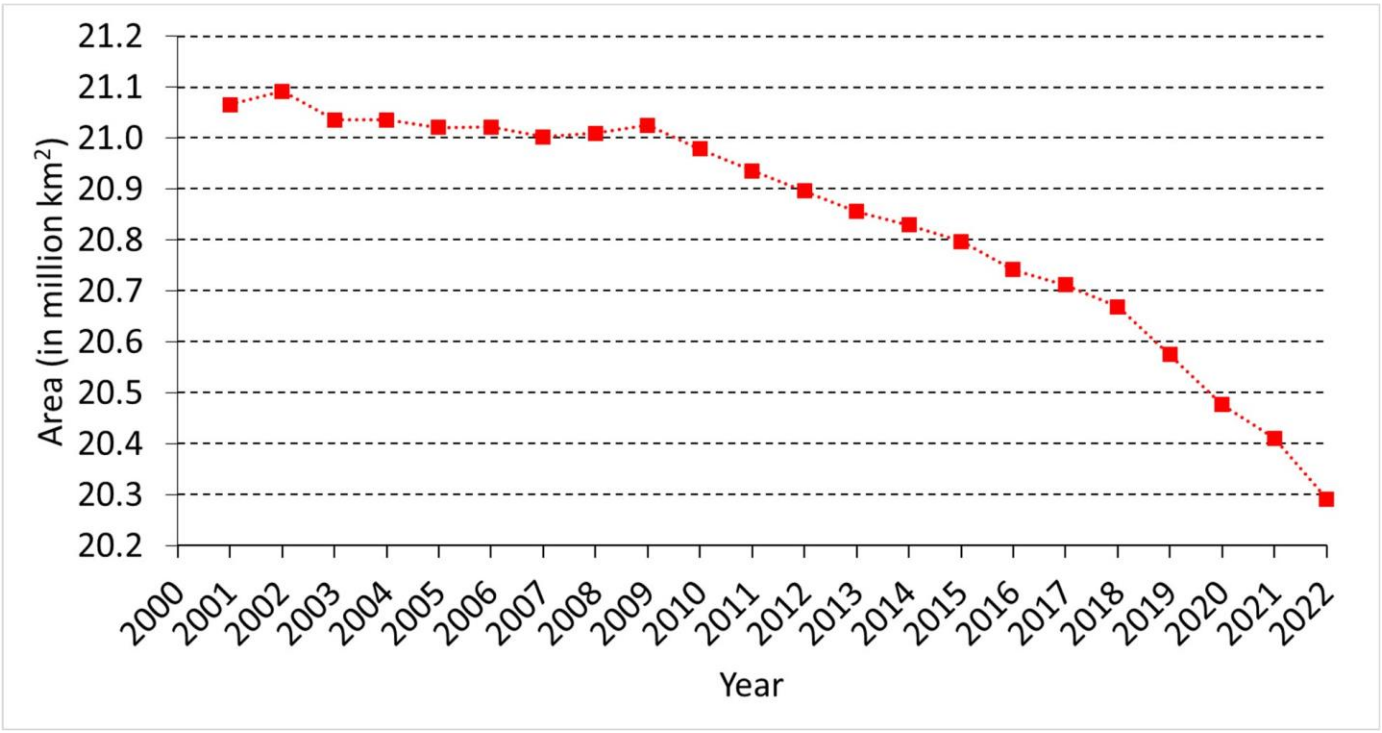

Figure 3. Global barren area per year.

The unchanged barren areas per continent ranges from 51,663 km^2 (Europe) to 9,769,208 km^2 (Africa) (Table 2). The transitional areas of Africa, Asia, Australia, Europe, North America, and South America cover 6.1%, 16.4%, 73.2%, 54.1%, 63.4%, and 21.2% of their MaxE extent, respectively.

Table 2. Total land surface area (km^2), unchanged (barren) area (km^2), and maximum extent of the barren area (km^2), per continent.

Continent	Total Area (km^2)	Unchanged Area (km^2)	Maximum Extent (km^2)
Africa	29,904,894	9,769,208	10,409,215
Asia	44,906,061	7,894,262	9,441,675
Australia	8,115,839	72,991	271,969
Europe	9,939,509	51,663	112,675
North America	24,266,604	452,960	1,236,318
South America	17,703,640	594,940	755,290

3.2. Transition Dynamics between Barren Areas and Other Land Cover Units

Regions characterized by a low transition occurrence (0–10% TO) account for a relatively large portion of the transitional areas (16.3%), meaning that these areas are predominantly barren areas (Figure 4). On the contrary, areas that predominantly consist of other land cover classes (90–100% TO) account for 30.6% of the transitional areas. The interannual changes in global barren areas are largely reflected by transitions to grasslands, open shrublands, permanent snow and ice, and water bodies (Figure 5). The remaining land cover classes have less than a 0.5% contribution to the barren transitions. Unchanged barren areas are mainly found between 15 ° N and 45 ° N longitude zones, while barren transitions to snow and ice and water bodies mainly occurred in the artic regions of the Northern Hemisphere. On the contrary, barren transitions to open shrublands were widely distributed between 45 ° N and 45 ° S latitude zones. Barren transitions to grasslands were found across different regions in the Northern Hemisphere. Barren transitions to a single land class between 2001 and 2022 accounted for 87.1% of the total transitional area, while barren transitions to two land classes covered 12.3% of the total transitional area. The remaining 0.6% is partitioned to barren transitions to three land cover classes. Barren to grassland, open shrublands transitions, permanent snow and ice, and water bodies are found to account for 50.3%, 26.6%, 8.3%, and 2.2% of the transitional area, respectively.

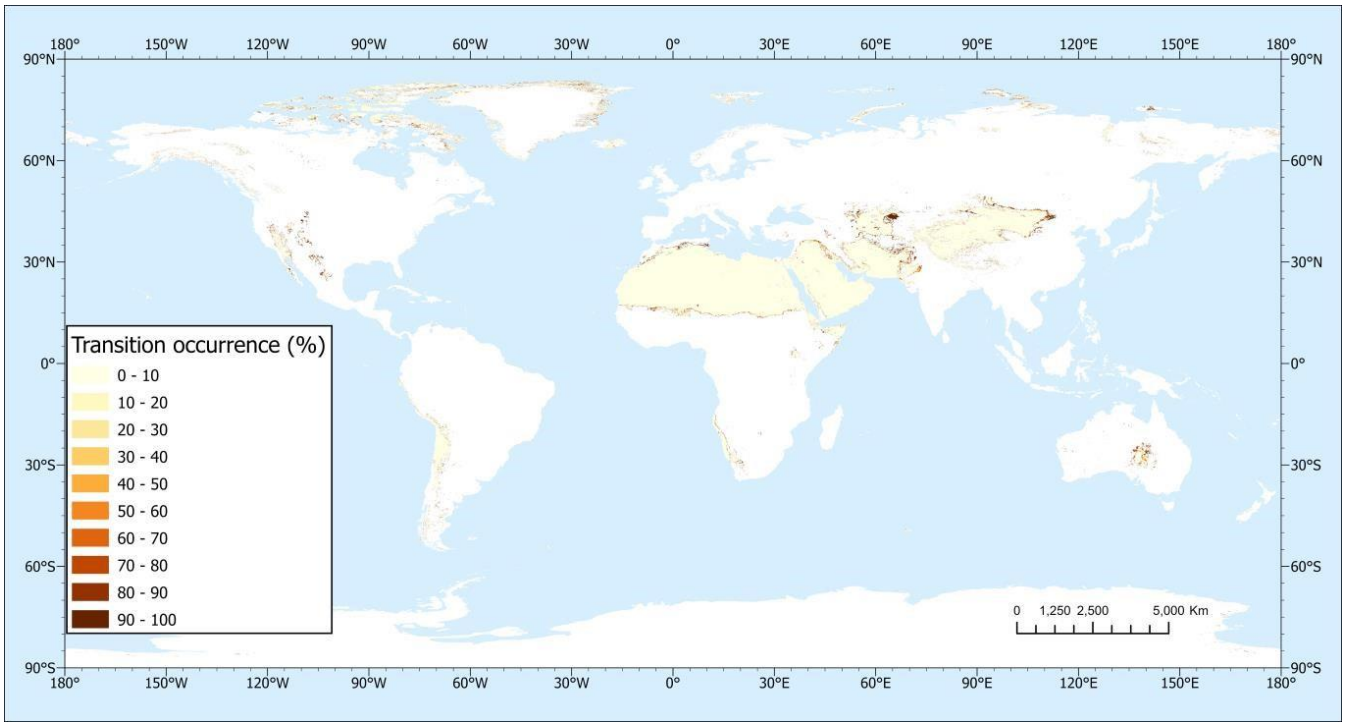

Figure 4. Transition occurrence of barren areas to other land cover classes.

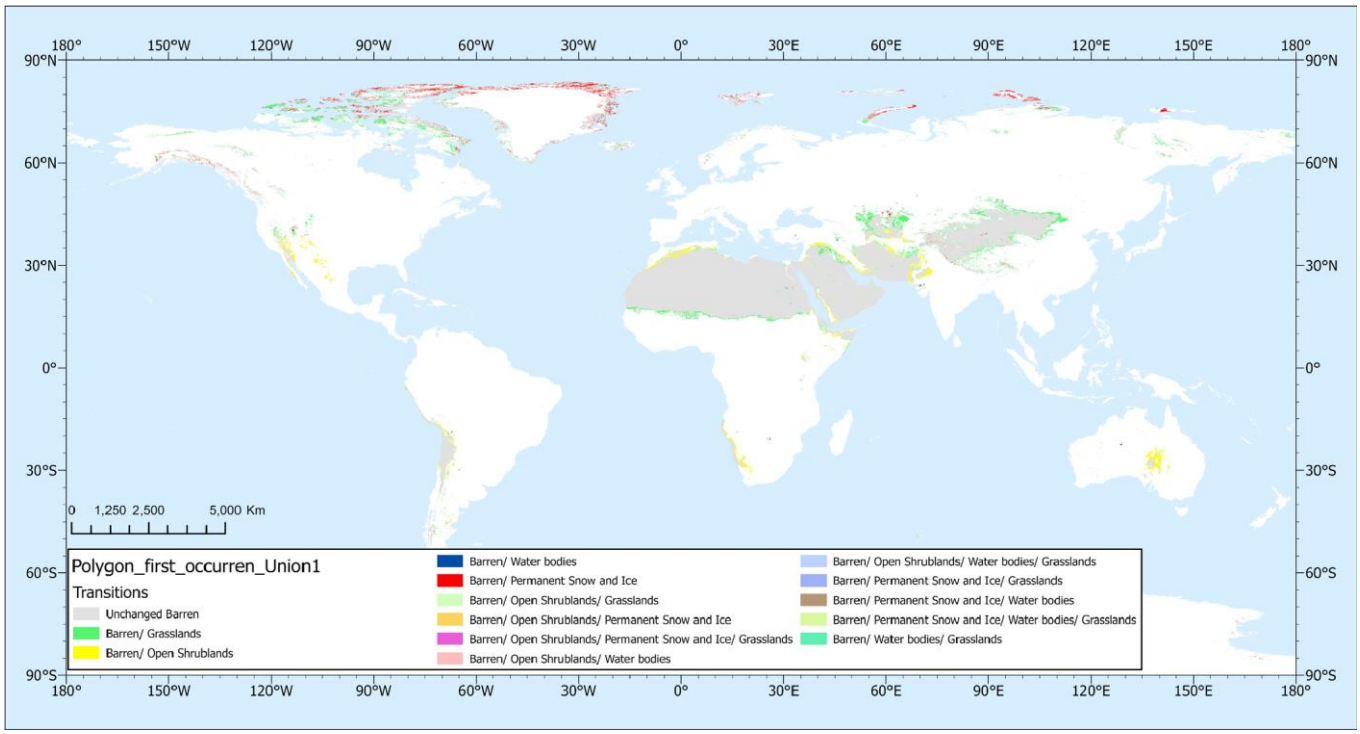

Figure 5. Spatial transitions of barren areas to other land cover classes.

The transitions between barren areas and other land cover classes are characterized by high interannual variability (Figure 6). Globally, barren areas show a gradual reduction from 2001 (91.1% of MaxE) to 2012 (86.8%), followed by annual fluctuations until 2022 (88.1%). Grasslands show a gradual increase from 2001 (4.0% of MaxE) to 2012 (7.4% of MaxE), followed by annual fluctuations until 2022 (6.4%). Open shrublands show a gradual increase from 2001 (1.5%) to 2005 (2.6%), followed by a gradual decline until 2009 (2.3%), a gradual increase until 2020 (3.0%), and a sharp decrease until 2022 (2.7%). Permanent snow and ice ranged between 1.9% (2001) and 2.9% (2018). A gradual decline in permanent snow and ice was observed from 2018 to 2022 (2.1%). Water bodies ranged from 0.3% (2001) to 0.5% (2016).

Figure 6. Global annual changes of the land cover over the maximum extent (MaxE) of barren area, expressed as percentages of the MaxE (*Y*-axis starts at 80% for better visualization of the land cover classes).

The highest relative interannual changes in barren areas were observed in Australia, ranging from 76.0% of MaxE (2009) to 33.9% of MaxE (2012) (Figure 7). Relatively high interannual changes were observed in Europe and North America (N. America), ranging from 79.8% (2002) to 67.6% (2010) and from 72.2% (2003) to 60.3% (2011), respectively. Asia had a sharp decline in the barren area distribution from 2001 (94.4%) to 2002 (91.7%), followed by a gradual decline until 2020 (86.9%) and a gradual increase until 2022 (88.8%). South America (S. America) and Africa showed relatively small changes in barren area from 2001 to 2022.

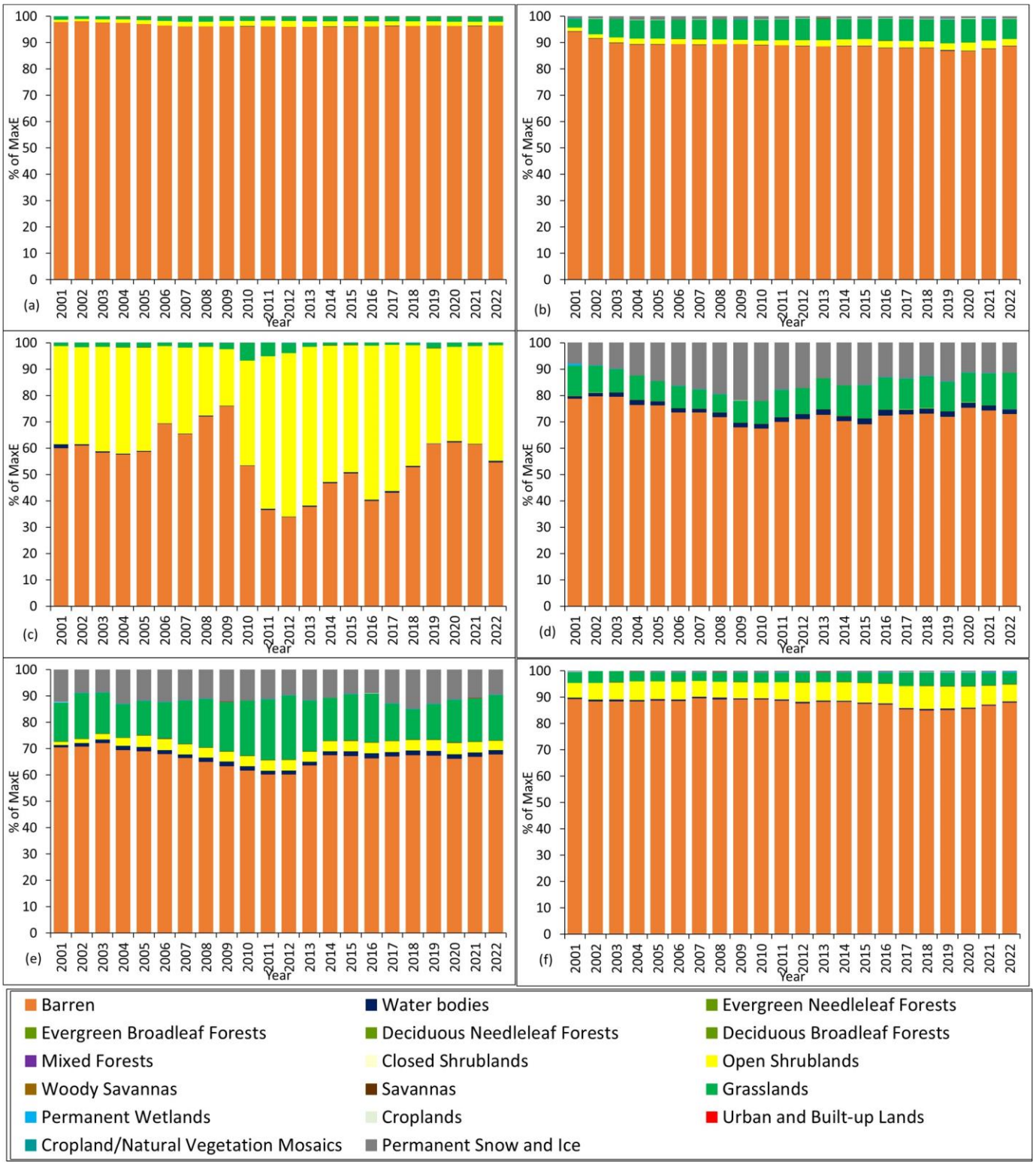

Figure 7. Annual changes in the land cover over the maximum extent (MaxE) of barren area, expressed as percentages of the MaxE, for Africa (**a**), Asia (**b**), Australia (**c**), Europe (**d**), North America (**e**), and South America (**f**).

The largest (unchanged) barren area worldwide is found to be in Africa (Appendix A, Figure A1), covering 33.3% of the total land surface (Table 2). Significant portions of barren areas are found in the Sahara and Namib and Kalahari deserts. The transitional area between the unchanged barren land and the maximum extent of the barren land (464,777 km^2) exhibited interchanges from barren to grasslands and open shrublands, and vice versa (Figure 7a). Open shrublands gradually increased from 2001 (0.8% of MaxE) to 2012 (2.2% of MaxE) and then gradually declined until 2022 (1.4% of MaxE). Similarly, grasslands increased from 2002 (0.8% of MaxE) to 2009 (1.9% of MaxE). Open shrublands and grasslands showed a similar gradual increase from 2002 to 2009. During the period between 2009 and 2022, the two classes revealed opposite fluctuations.

Asia's unchanged barren area is found to be equal to 18.4% of Asia's total land surface area. Barren areas are also found in the Arabian Peninsula, Iran, Thar, Gobi, and Taklamakan (Appendix A, Figure A2). The transitional area (1,168,426 km^2) consists mainly of interchanges from barren to grasslands and, to a smaller extent, from barren to open shrublands and snow and ice (Figure 7b). Grasslands showed a sharp increase from 2001 (3.3% of MaxE) to 2003 (7.0% of MaxE), followed by a gradual increase until 2020 (8.9% of MaxE) and a gradual decline until 2022 (7.6% of MaxE). A similar trend was observed for the open shrublands. On the contrary, snow and ice decreased from 2004 (1.3% of MaxE) to 2022 (0.9% of MaxE).

The barren area in Australia represents about 1.4% of the continent's total land surface (Appendix A, Figure A3). An area covering 162,039 km^2 was interchanging mainly from barren to open shrubland, and vice versa (Figure 7c). Open shrublands showed a gradual decrease from 2001 (37.3% of MaxE) to 2009 (21.5% of MaxE), followed by a sharp increase until 2012 (62.0% of MaxE). For the period 2013 to 2022, the MaxE of open shrublands ranged from 60.3 (2013) to 35.8% (2020), whereas grasslands showed a sharp increase between 2009 (2.3% of MaxE) and 2010 (6.6% of MaxE), followed by a gradual decline until 2022 (1.2% of MaxE).

Europe possessed the smallest barren area, found to be 0.7% of its total land surface (Appendix A, Figure A4). Barren areas mainly occurred in the northern and arctic regions (e.g., Scandinavia, Iceland), and in high elevations (Alps). As expected, the main portion of the barren areas is attributed to interchanges between snow and ice, and at a smaller extent, with grasslands (Figure 7d). Snow and ice land cover peaked in 2010 (23.5% of MaxE) and gradually declined until 2022 (12.9% of MaxE). Grasslands gradually declined until 2009 (7.0%), followed by a gradual increase until 2015 (12.6%), relatively small changes until 2021 (12.2%), and a sharp increase in 2022 (13.8%).

North America's barren area is found to possess around 2.6% of its total land surface. Barren areas are also found in the arctic region and the Great Basin, Mojave, Chihuahuan, and Sonoran Desert regions (Appendix A, Figure A5). In an area of 600,744 km^2, barren areas were transposing to grasslands and snow and ice, and vice versa (Figure 7e). The presence of grasslands increased from 12.7% of MaxE (2004) to 24.4% of MaxE (2012), followed by a gradual decline until 2018 (11.5% of MaxE) and an increase in 2022 (17.2% of MaxE). In addition, barren areas covered by either snow or ice ranged from 9.8 (2003) to 16.4% (2018).

South America's barren area is equal to 3.6% of its total land surface and is found mainly in the Atacama and Patagonia regions (Appendix A, Figure A6). In the transitional area of 125,495 km^2, barren areas were interchanging mainly between open shrublands and grasslands (Figure 7f). Open shrublands ranged from 5.4% of MaxE (2001) to 8.6% of MaxE (2018), and grasslands ranged from 3.1% of MaxE (2007) to 5.0% of MaxE (2017).

4. Discussion

The use of the maximum extent of barren areas (MaxE) in this study allowed the in-depth analysis of the spatial extent of the barren areas and their temporal dynamics. This study showed an overall decrease of 3.7% of global barren areas between 2001 and 2022. Our findings are consistent with the decreasing barren area trends and transition patterns found in previous studies [10,22,24,25]. In their recent study on the spatiotemporal analysis of land cover at global scale, Jing et al. [10] reported a year-by-year decrease in global barren areas for 2001–2022, possibly related to human activities such as reforestation and grassland restoration. Similarly, Wu et al. [23] showed that the majority of the barren areas across the globe had decreasing trends from 2000 to 2019. Song et al. [24] reported a decrease in global barren areas by 1.16 million km^2 (3.1%) from 1982 to 2016, whereas Lamchin et al. [25] estimated a reduction of 0.06% from 1992 to 2018. The discrepancies found in the magnitude of the global barren area reduction among the existing studies are mainly attributed to the analysis of different monitoring periods and due to the use of different satellite products (e.g., AVHRR, Landsat, MODIS), which offer different spatial resolutions.

Barren transitional areas, which cover an area of 3,438,959 km^2, showed land cover changes to other classes in the following magnitude order: grasslands, open shrublands, snow and ice, and water bodies. These results are in agreement with the findings of Jing et al. [10], who showed similar transitions between barren and grasslands, open shrublands, and permanent snow and ice. Similarly, Liu et al. [22] showed relatively high transitions of grasslands, shrublands, and tundra to

barren areas, and vice versa. However, they also found a high contribution of croplands, which differs from the results of this study.
Transitions between barren and cropland in this study ranged between 0.03% (2002) and 0.09% (2020).

The present study focused explicitly on quantifying the spatiotemporal dynamics of barren areas and their transitions to other land cover classes, thus no analysis has been conducted on the driving factors that lead to these spatiotemporal changes. These transitions can be attributed to various factors such as environmental (e.g., ecological fragility), anthropogenic (e.g., weak governance, poverty), and climate change. Previous studies have shown that barren lands in the Arctic exhibited noticeable transitions to grasslands and barren land, due to global warming [10,22]. Additionally, climate change has led to degradation and desertification of large areas over eastern and central Asia [26,27] and North Africa [28]. Indeed, all these regions were identified as barren area hotspots in the present study. In their study on the responses of vegetation to climate variables over global drylands from 1985 to 2015, He et al. [29] found that the annual variations in global land cover (expressed in the Normalized Difference Vegetation Index) were primarily affected by the precipitation in the dryland regions in Africa, Australia, East Asia, South Asia, and North America. Temperature had an impact on drylands in southern South Asia; northern Australia; small areas of Africa, West Asia, and Europe; and high-latitude drylands in the Northern Hemisphere. Potential evapotranspiration could explain the variations in drylands of the remaining regions. On the contrary, Song et al. [24] reported that land use activities account for the majority of observed land changes in Europe (86%), South America (66%), Asia (62%), and Africa (50%), but have a smaller role in North America
(47%) and Oceania (35%). These contrasting results on the driving factors responsible for the changes in land cover provide an excellent research opportunity for future studies on this topic.

5. Conclusions

This study examined the spatiotemporal changes in barren areas on global and continental scales from 2001 to 2022 using geospatial analysis and MODIS land cover products and by introducing the MaxE concept, which is computed by extracting the barren information from multidimensional data across all slices of the temporal dimension (time instants). The main conclusions drawn from this study are the following:

- The use of MaxE provided the opportunity to conduct detailed analysis of the spatiotemporal changes, as any annual change observed in the barren distribution was comparable over the entire dataset.
- A large portion of the barren areas remained unchanged for 22 years. This portion is equivalent to 12.8% of the global land surface area. However, the results indicated a 3.7% decrease in global barren areas from 2001 to 2022, mainly due to transitions to grasslands and open shrublands.
- Barren transitional areas, which constitute approximately 2.3% of the global land surface area, are found to be highly dynamic both in space and time. Different barren transitions were found for different regions of the world. Particularly, transitions to open shrublands can be found in the majority of the barren regions, whereas grasslands are mostly limited to the Northern Hemisphere. Barren areas that are present in the artic regions revealed interchanges, mainly between snow and ice and water bodies. On a global scale, barren to grassland, open shrublands transitions, permanent snow and ice, and water bodies account for 50.3%, 26.6%, 8.3% and 2.2% of the transitional area, respectively. Barren transitional areas are also found to exhibit strong temporal variations, as shown by their high relative changes over time.
- The fragility of some ecosystems has been revealed, as areas that predominantly consist of other land cover classes (90–100% TO) account for 30.6% of the transitional areas. Also, this study identified emerging barren hotspot areas in the Mangystau region (Kazakhstan), the Tibetan plateau, Northern Greenland, and the Atlas Mountains, which is in agreement with recent published studies on land changes in these regions. Up-to-date information on the land cover will provide the opportunity to monitor the evolution of these regions.

Overall, this study provides in-depth information on the spatiotemporal evolution of the global barren areas. Future research relating the outcomes of this study to the driving factors

causing barren changes will be extremely valuable towards understanding and predicting future changes.

Author Contributions: Conceptualization, M.E.; methodology, validation, formal analysis, M.E., S.N., M.N.A., M.M., I.V. and C.F.P.; investigation, software, resources, data curation, M.E. and S.N.; writing—original draft preparation, M.E.; writing—review and editing, M.E., C.F.P., C.P., F.B., I.V., M.N.A., S.N., S.M. and D.H.; visualization, M.E. and S.N.; supervision, S.M. and D.H.; project administration, D.H.; funding acquisition, D.H. All authors have read and agreed to the published version of the manuscript.

Funding: This research was funded by the 'EXCELSIOR' project (European Union's Horizon 2020 research and innovation programme), grant number "857510", and "The APC was funded by Remote Sensing MDPI by providing full waive for the paper publication".

Data Availability Statement: The MODIS data products are contained within this article and were extracted from the NASA EARTHDATA webpage (https://lpdaac.usgs.gov/products/mcd12c1v061, accessed on 9 January 2024).

Acknowledgments: The authors acknowledge the "EXCELSIOR": ERATOSTHENES: Excellence Research Centre for Earth Surveillance and Space-Based Monitoring of the Environment H2020 Widespread Teaming project (www.excelsior2020.eu, accessed on 9 January 2024). The "EXCELSIOR" project has received funding from the European Union's Horizon 2020 Research and Innovation Programme under Grant Agreement No. 857510, from the Government of the Republic of Cyprus through the Directorate General for the European Programmes, Coordination and Development and the Cyprus University of Technology.

Conflicts of Interest: The authors declare no conflicts of interest.

Appendix A

Maps of the Unchanged (UA) and Transitional (TA) Barren Areas Per Continent

Figure A1. Unchanged (yellow) and transitional (red) barren areas in Africa.

Figure A2. Unchanged (yellow) and transitional (red) barren areas in Asia.

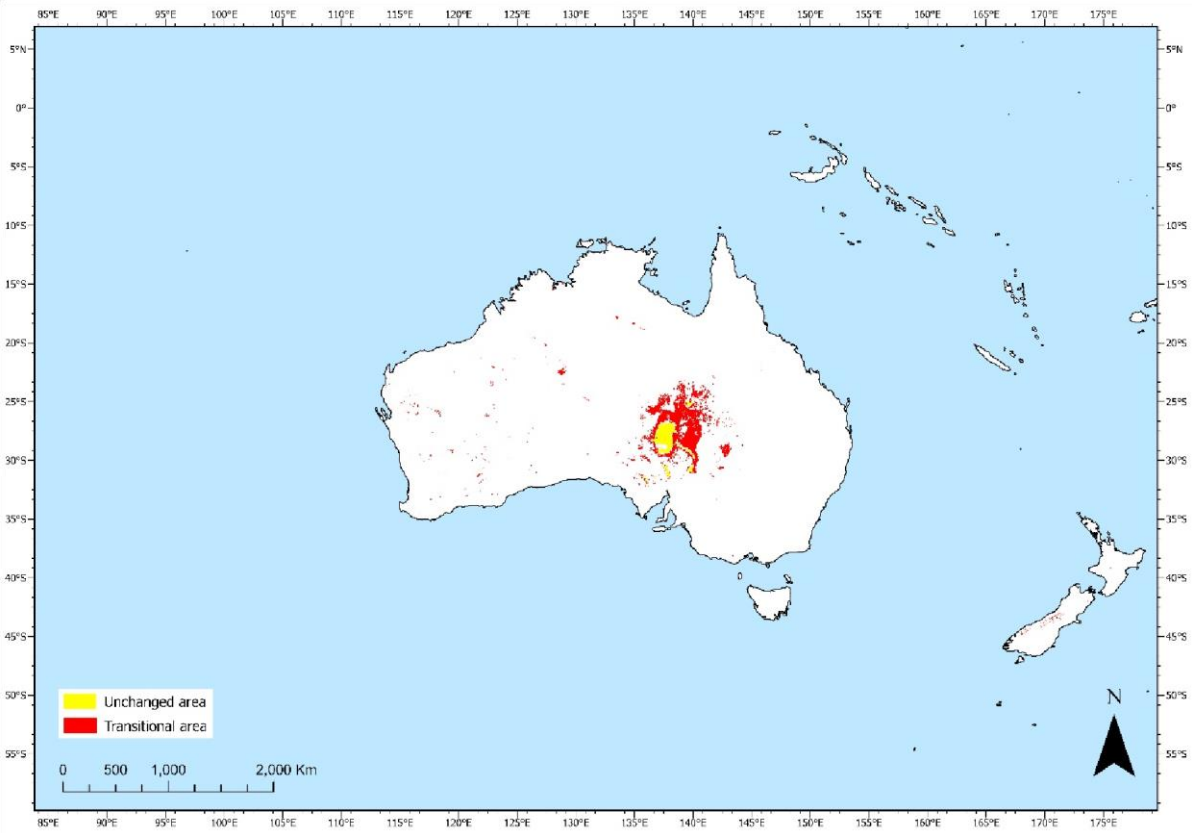

Figure A3. Unchanged (yellow) and transitional (red) barren areas in Australia.

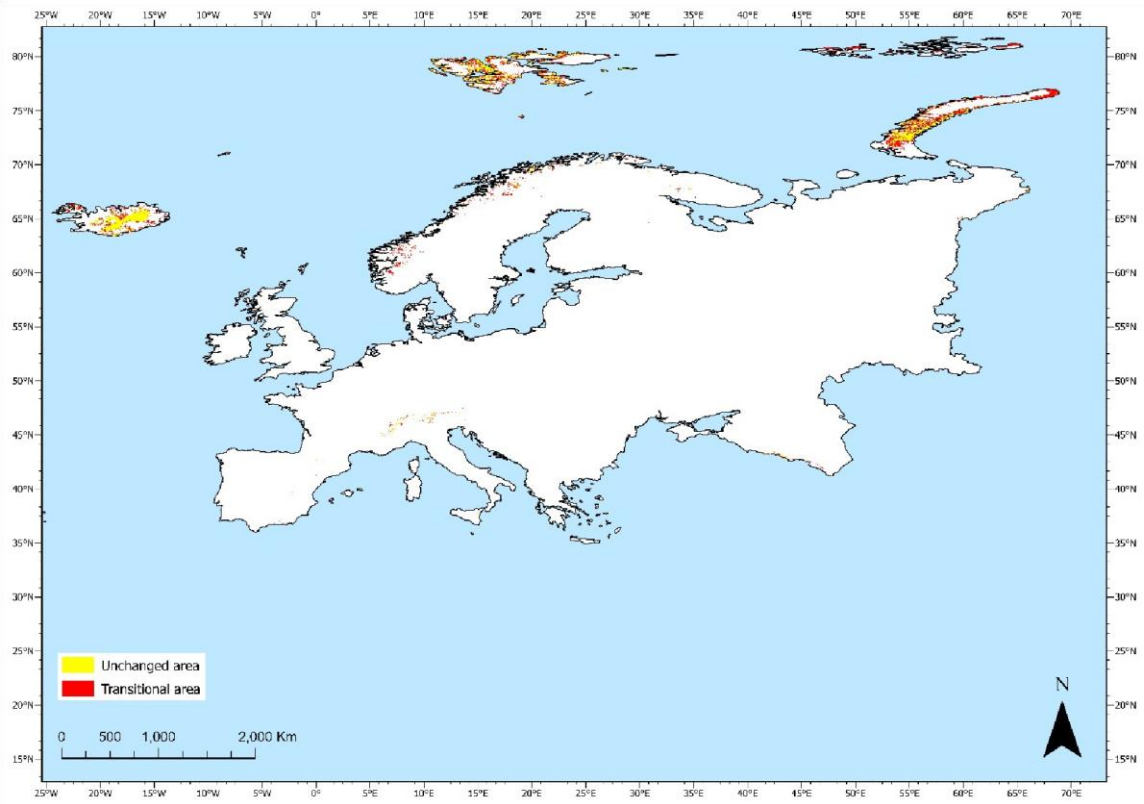

Figure A4. Unchanged (yellow) and transitional (red) barren areas in Europe.

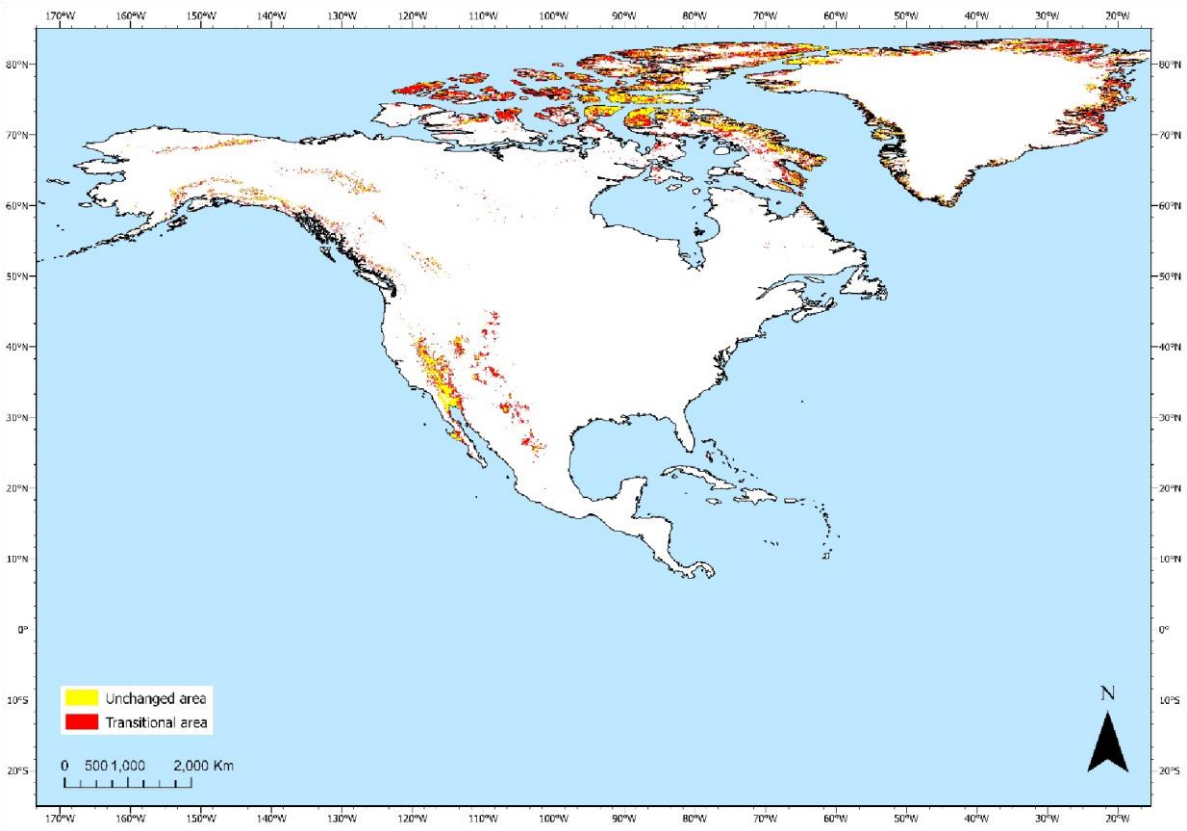

Figure A5. Unchanged (yellow) and transitional (red) barren areas in North America.

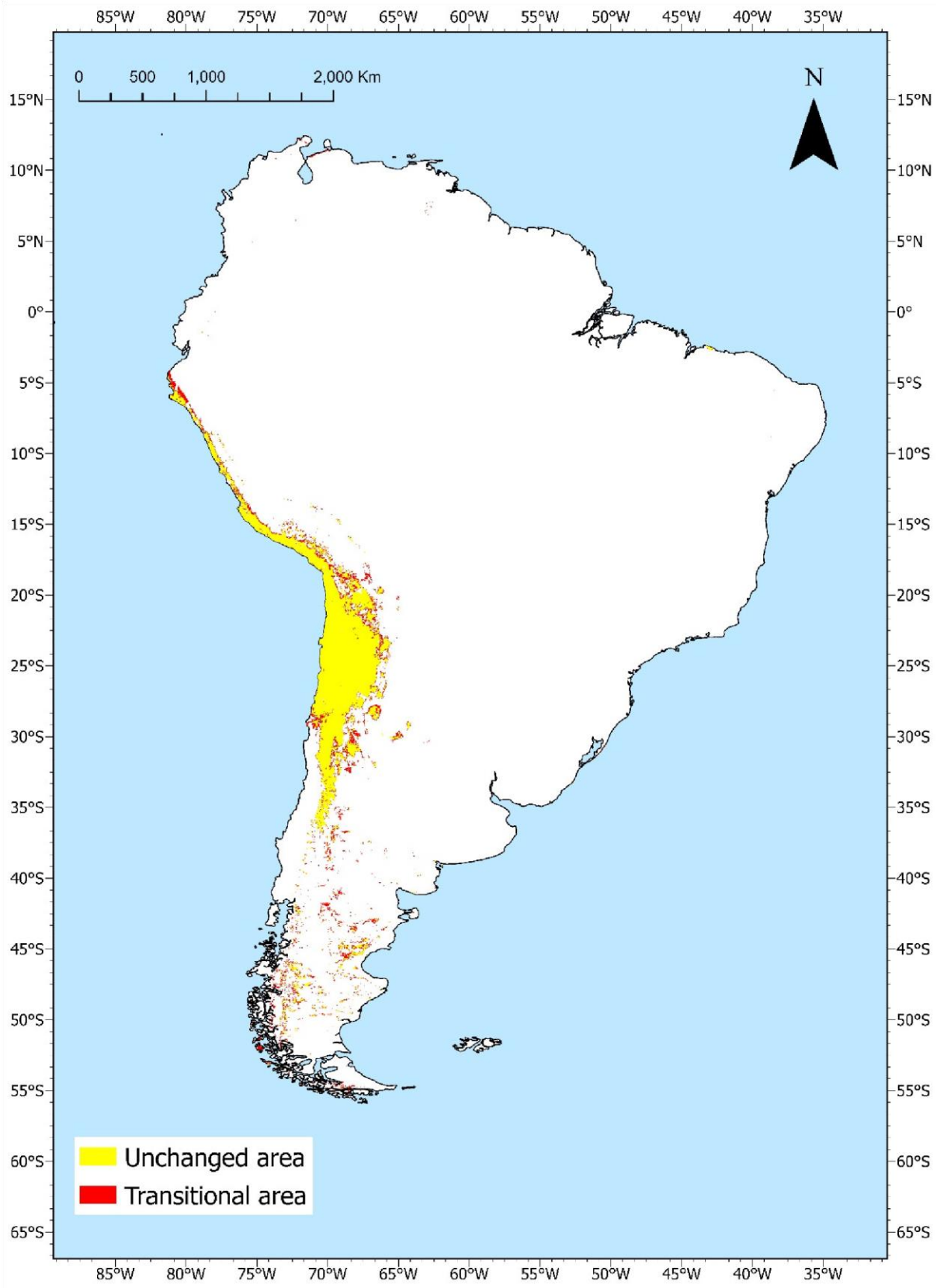

Figure A6. Unchanged (yellow) and transitional (red) barren areas in South America.

References

1. Wang, Z.; Wu, J.; Niu, B.; He, Y.; Zu, J.; Li, M.; Zhang, X. Vegetation Expansion on the Tibetan Plateau and Its Relationship with Climate Change. *Remote Sens.* **2020**, *12*, 4150. [CrossRef]
2. Ding, Y.; Feng, Y.; Chen, K.; Zhang, X. Analysis of Spatial and Temporal Changes in Vegetation Cover and Its Drivers in the Aksu River Basin, China. *Sci. Rep.* **2024**, *14*, 10165. [CrossRef] [PubMed]
3. Dasgupta, B.; Sanyal, P. Linking Land Use Land Cover Change to Global Groundwater Storage. *Sci. Total Environ.* **2022**, *853*, 158618. [CrossRef] [PubMed]

4. Eliades, M.; Michaelides, S.; Evagorou, E.; Fotiou, K.; Fragkos, K.; Leventis, G.; Theocharidis, C.; Panagiotou, C.F.; Mavrovouniotis, M.; Neophytides, S.; et al. Earth Observation in the EMMENA Region: Scoping Review of Current Applications and Knowledge Gaps. *Remote Sens.* **2023**, *15*, 4202. [CrossRef]
5. Pandey, P.C.; Koutsias, N.; Petropoulos, G.P.; Srivastava, P.K.; Ben Dor, E. Land Use/Land Cover in View of Earth Observation: Data Sources, Input Dimensions, and Classifiers—A Review of the State of the Art. *Geocarto Int.* **2021**, *36*, 957–988. [CrossRef] 6. Buchhorn, M.; Lesiv, M.; Tsendbazar, N.-E.; Herold, M.; Bertels, L.; Smets, B. Copernicus Global Land Cover Layers—Collection 2. *Remote Sens.* **2020**, *12*, 1044. [CrossRef]
7. Friedl, M.A.; Sulla-Menashe, D.; Tan, B.; Schneider, A.; Ramankutty, N.; Sibley, A.; Huang, X. MODIS Collection 5 Global Land Cover: Algorithm Refinements and Characterization of New Datasets. *Remote Sens. Environ.* **2010**, *114*, 168–182. [CrossRef] 8. Phiri, D.; Simwanda, M.; Salekin, S.; Nyirenda, V.R.; Murayama, Y.; Ranagalage, M. Sentinel-2 Data for Land Cover/Use Mapping: A Review. *Remote Sens.* **2020**, *12*, 2291. [CrossRef]
9. Zhang, C.; Li, X. Land Use and Land Cover Mapping in the Era of Big Data. *Land* **2022**, *11*, 1692. [CrossRef]
10. Jing, Q.; He, J.; Li, Y.; Yang, X.; Peng, Y.; Wang, H.; Yu, F.; Wu, J.; Gong, S.; Che, H.; et al. Analysis of the Spatiotemporal Changes in Global Land Cover from 2001 to 2020. *Sci. Total Environ.* **2024**, *908*, 168354. [CrossRef]
11. Zhang, X.; Zhao, T.; Xu, H.; Liu, W.; Wang, J.; Chen, X.; Liu, L. GLC_FCS30D: The First Global 30 m Land-Cover Dynamics Monitoring Product with a Fine Classification System for the Period from 1985 to 2022 Generated Using Dense-Time-Series Landsat Imagery and the Continuous Change-Detection Method. *Earth Syst. Sci. Data* **2024**, *16*, 1353–1381. [CrossRef]
12. Nie, T.; Dong, G.; Jiang, X.; Lei, Y. Spatio-Temporal Changes and Driving Forces of Vegetation Coverage on the Loess Plateau of Northern Shaanxi. *Remote Sens.* **2021**, *13*, 613. [CrossRef]
13. Zhai, H.; Lv, C.; Liu, W.; Yang, C.; Fan, D.; Wang, Z.; Guan, Q. Understanding Spatio-Temporal Patterns of Land Use/Land Cover Change under Urbanization in Wuhan, China, 2000–2019. *Remote Sens.* **2021**, *13*, 3331. [CrossRef]
14. Youssef, Y.M.; Gemail, K.S.; Atia, H.M.; Mahdy, M. Insight into Land Cover Dynamics and Water Challenges under Anthropogenic and Climatic Changes in the Eastern Nile Delta: Inference from Remote Sensing and GIS Data. *Sci. Total Environ.* **2024**, *913*, 169690. [CrossRef]
15. Chowdhury, M.; Hasan, M.E.; Abdullah-Al-Mamun, M.M. Land Use/Land Cover Change Assessment of Halda Watershed Using Remote Sensing and GIS. *Egypt. J. Remote Sens. Space Sci.* **2020**, *23*, 63–75. [CrossRef]
16. Faruque, M.J.; Vekerdy, Z.; Hasan, M.Y.; Islam, K.Z.; Young, B.; Ahmed, M.T.; Monir, M.U.; Shovon, S.M.; Kakon, J.F.; Kundu, P. Monitoring of Land Use and Land Cover Changes by Using Remote Sensing and GIS Techniques at Human-Induced Mangrove Forests Areas in Bangladesh. *Remote Sens. Appl. Soc. Environ.* **2022**, *25*, 100699. [CrossRef]
17. Quamar, M.M.; Al-Ramadan, B.; Khan, K.; Shafiullah, M.; El Ferik, S. Advancements and Applications of Drone-Integrated Geographic Information System Technology—A Review. *Remote Sens.* **2023**, *15*, 5039. [CrossRef]
18. Kumar, M.; Singh, R.B.; Singh, A.; Pravesh, R.; Majid, S.I.; Tiwari, A. (Eds.) Introduction of Geographic Information System. In *Geographic Information Systems in Urban Planning and Management*; Springer Nature: Singapore, 2023; pp. 3–24. ISBN 978-98119785-5-5.
19. Brown, A.G.; Tooth, S.; Bullard, J.E.; Thomas, D.S.G.; Chiverrell, R.C.; Plater, A.J.; Murton, J.; Thorndycraft, V.R.; Tarolli, P.; Rose, J.; et al. The Geomorphology of the Anthropocene: Emergence, Status and Implications. *Earth Surf. Process. Landf.* **2017**, *42*, 71–90. [CrossRef]
20. Wang, H.; Liu, Y.; Wang, Y.; Yao, Y.; Wang, C. Land Cover Change in Global Drylands: A Review. *Sci. Total Environ.* **2023**, *863*, 160943. [CrossRef]
21. Winkler, K.; Fuchs, R.; Rounsevell, M.; Herold, M. Global Land Use Changes Are Four Times Greater than Previously Estimated. *Nat. Commun.* **2021**, *12*, 2501. [CrossRef]
22. Liu, H.; Gong, P.; Wang, J.; Clinton, N.; Bai, Y.; Liang, S. Annual Dynamics of Global Land Cover and Its Long-Term Changes from 1982 to 2015. *Earth Syst. Sci. Data* **2020**, *12*, 1217–1243. [CrossRef]
23. Wu, S.; Liu, L.; Li, D.; Zhang, W.; Liu, K.; Shen, J.; Zhang, L. Global Desert Expansion during the 21st Century: Patterns, Predictors and Signals. *Land Degrad. Dev.* **2023**, *34*, 377–388. [CrossRef]
24. Song, X.-P.; Hansen, M.C.; Stehman, S.V.; Potapov, P.V.; Tyukavina, A.; Vermote, E.F.; Townshend, J.R. Global Land Change from 1982 to 2016. *Nature* **2018**, *560*, 639–643. [CrossRef] [PubMed]
25. Lamchin, M.; Bilintoh, T.M.; Lee, W.-K.; Ochir, A.; Lim, C.-H. Exploring Spatio-Temporal Change in Global Land Cover Using Categorical Intensity Analysis. *Front. For. Glob. Chang.* **2022**, *5*, 994713. [CrossRef]
26. Hu, Y.; Han, Y.; Zhang, Y. Land Desertification and Its Influencing Factors in Kazakhstan. *J. Arid Environ.* **2020**, *180*, 104203. [CrossRef]
27. Chen, Y.; Xu, E. The Spatiotemporal Change in Land Cover and Discrepancies within Different Countries on the Qinghai–Tibet Plateau over a Recent 30-Year Period. *Land* **2023**, *12*, 1797. [CrossRef]
28. El Hairchi, K.; Ben Brahim, Y.; Ouiaboub, L.; Limame, A.; Saadi, O.; Nouayti, A. Desertification Modeling in the Moroccan Middle Atlas Using Sentinel-2A Images and TCT Indexes (Case of the Ain Nokra Forest). *Model. Earth Syst. Environ.* **2023**, *9*, 4279–4293. [CrossRef]
29. He, L.; Guo, J.; Yang, W.; Jiang, Q.; Chen, L.; Tang, K. Multifaceted Responses of Vegetation to Average and Extreme Climate Change Over Global Drylands. *Sci. Total Environ.* **2023**, *858*, 159942. [CrossRef]

Disclaimer/Publisher's Note: The statements, opinions and data contained in all publications are solely those of the individual author(s) and contributor(s) and not of MDPI and/or the editor(s). MDPI and/or the editor(s) disclaim responsibility for any injury to people or property resulting from any ideas, methods, instructions or products referred to in the content.